Persistent DNA-break potential near telomeres increases initiation of meiotic recombination on small chromosomes

Vijayalakshmi V. Subramanian[1], Tovah E. Markowitz[1], Luis A. Vale-Silva[1], Pedro A. San-Segundo[2], Nancy M. Hollingsworth[3], and Andreas Hochwagen[1*]

[1] Department of Biology, New York University, New York, NY 10003, USA

[2] Instituto de Biología Funcional y Genómica, Consejo Superior de Investigaciones Científicas, and University of Salamanca, 37007 Salamanca, Spain

[3] Department of Biochemistry and Cell Biology, Stony Brook University, Stony Brook, NY 11794, USA

* Correspondence: andi@nyu.edu

Running title: Regional control of meiotic DNA breakage

SUMMARY

Faithful meiotic chromosome inheritance and fertility relies on the stimulation of meiotic crossover recombination by potentially genotoxic DNA double-strand breaks (DSBs). To avoid excessive damage, feedback mechanisms down-regulate DSBs on chromosomes that have successfully initiated crossover repair. In *Saccharomyces cerevisiae*, this regulation requires the removal of the conserved DSB-promoting protein Hop1/HORMAD during chromosome synapsis. Here, we identify privileged domains spanning roughly 100 Kb near all telomeres that escape this regulation and continue to break in pachynema, well after chromosomes are fully synapsed. These telomere-adjacent regions (TARs) retain Hop1 despite normal synapsis, indicating that synapsis is necessary but not sufficient for Hop1 removal. TAR establishment requires the disassemblase Pch2/TRIP13, which preferentially removes Hop1 from telomere-distant sequences. Importantly, the uniform size of TARs between chromosomes contributes to disproportionately high DSB and repair signals on small chromosomes in pachynema, suggesting that TARs partially underlie the curiously high recombination rate of small chromosomes.

INTRODUCTION

Meiosis generates haploid sex cells using two consecutive chromosome segregation events that follow a single cycle of DNA replication (Kleckner, 1996; Moore and Orr-Weaver, 1998; Page and Hawley, 2003; Petronczki et al., 2003). To assist proper separation of the homologous chromosomes in the first segregation phase (meiosis I), numerous DNA double-stranded breaks (DSBs) are introduced to stimulate the formation of crossover recombination products (COs) (de Massy, 2013; Hunter, 2015; Lam and Keeney, 2014). Together with sister chromatid cohesion, COs connect homologous chromosome pairs and promote their correct alignment on the meiosis I spindle (Bickel et al., 2002; Buonomo et al., 2000; Kudo et al., 2006; Lee and Orr-Weaver, 2001; van Heemst and Heyting, 2000).

Because DSBs are potentially genotoxic, a number of processes choreograph DSB formation at the right place and time to maintain genome integrity (Cooper et al., 2016; de Massy, 2013; Gray and Cohen, 2016; Lam and Keeney, 2014; Subramanian and Hochwagen, 2014; Yu et al., 2016). Induction of meiotic DSBs is catalyzed by the topoisomerase-like Spo11 enzyme and occurs predominantly at DSB hotspots (Baudat and Nicolas, 1997; Blitzblau et al., 2007; Buhler et al., 2007; Gerton et al., 2000; Pan et al., 2011). Spo11 is modulated by chromatin structure and is strongly dependent on the specialized loop-axis architecture of meiotic chromosomes to generate DSBs (Blat et al., 2002; Borde and de Massy, 2013; Panizza et al., 2011; Sommermeyer et al., 2013). While DSB hotspots are primarily found on the loops, several Spo11 accessory proteins are located on the meiotic chromosome axis (Kumar et al., 2010; Miyoshi et al., 2012; Panizza et al., 2011). Hotspots are thought to translocate to the axis for DSB formation (Blat et al., 2002; Borde and de Massy, 2013; Panizza et al., 2011). Consistent with a stimulatory role of axis protein in DSB formation, axis protein mutants exhibit severely reduced DSB levels (Goodyer et al., 2008; Kim et al., 2010; Kim et al., 2014; Kumar et al., 2015; Mao-Draayer et al., 1996; Mehrotra and McKim, 2006; Mets and Meyer, 2009; Wojtasz et al., 2009; Xu et al., 1997) and the local enrichment of axis proteins correlates well with DSB levels (Panizza et al., 2011; Sun et al., 2015).

In addition to the spatial regulation of Spo11 activity, a network of checkpoint mechanisms controls the timing of DSB formation (Cooper et al., 2016; Subramanian and Hochwagen, 2014). These mechanisms prevent DSB formation during pre-meiotic DNA replication and after exit from meiotic prophase (Blitzblau and Hochwagen, 2013; Gray et al., 2013; Miyoshi et al., 2012; Murakami and Keeney, 2014; Ogino and Masai, 2006; Tonami et al., 2005). Checkpoint

mechanisms also suppress redundant DSB formation in the vicinity of already broken DNA (Garcia et al., 2015; Zhang et al., 2011). Moreover, DSB formation is down-regulated in a chromosome-autonomous fashion in response to initiation of CO repair with the homologue (Subramanian et al., 2016; Thacker et al., 2014; Wojtasz et al., 2009). This down-regulation is thought to ensure that DSB formation ceases only after each homologue pair has initiated formation of the obligatory CO.

Studies suggest that the synaptonemal complex (SC), an evolutionarily conserved proteinaceous structure that progressively assembles between homologous chromosomes, is responsible for chromosome-autonomous down-regulation of DSB formation (Subramanian et al., 2016; Thacker et al., 2014; Wojtasz et al., 2009). In *S. cerevisiae*, SC-dependent loss of DSB activity is linked to the chromosomal reduction of the axis-associated HORMA-domain protein Hop1 (Borner et al., 2008; San-Segundo and Roeder, 1999; Subramanian et al., 2016), which normally recruits DNA break machinery to the meiotic chromatin (Panizza et al., 2011). Hop1 removal from chromosomes occurs concomitantly with SC assembly and depends on SC-mediated recruitment of the AAA^{+}-ATPase Pch2 (Borner et al., 2008; San-Segundo and Roeder, 1999; Subramanian et al., 2016). In the absence of Pch2, Hop1 continues to accumulate on chromosome spreads in late prophase. A similar process is observed in mouse spermatocytes (Kumar et al., 2015; Wojtasz et al., 2009). Intriguingly, not all yeast DSB hotspots are equally dampened in late prophase. A number of DSB hotspots, including several that are widely used as model hotspots (e.g. *HIS4LEU2, YCR047c*), remain active irrespective of the presence of the SC (Allers and Lichten, 2001; Subramanian et al., 2016; Xu et al., 1995). The origin and purpose of these long-lived hotspots is not known.

One possible function of long-lived hotspots may be to increase the window of opportunity for DSB formation for small chromosomes. Small chromosomes exhibit elevated recombination density in many organisms (Backstrom et al., 2010; Blitzblau et al., 2007; Chakraborty et al., 2017; Gerton et al., 2000; Kaback, 1996; Kaback et al., 1992; Kaback et al., 1989; Lam and Keeney, 2015; Pan et al., 2011; Thacker et al., 2014). In yeast, this effect is likely driven by two independent mechanisms, both of which remain poorly understood. The first mechanism causes a biased enrichment of axis proteins and DSB factors on small chromosomes and is independent of DSB formation (Panizza et al., 2011; Sun et al., 2015). The second mechanism is thought to involve the chromosome-autonomous down-regulation of DSBs linked to successful CO designation (Thacker et al., 2014). It has been proposed that smaller

chromosomes may be slower at engaging with their homologue, leading to prolonged DSB activity specifically on these chromosomes (Thacker et al., 2014). Accordingly, in *zip3* mutants, which fail to designate DSBs for controlled CO repair (Fung et al., 2004; Serrentino et al., 2013), DSB formation continues on all chromosomes, and the biased increase in DSB levels on small chromosomes is no longer detectable (Thacker et al., 2014). This model, however, is likely incomplete because it predicts that long-lived hotspots will be restricted to small chromosomes. Instead, long-lived hotspots are also observed on large chromosomes (Subramanian et al., 2016).

Here, we show that most long-lived hotspots are located within large telomere-adjacent regions (TARs) that retain Hop1 and DSB markers in late prophase. Establishment of TARs requires Pch2, which preferentially removes Hop1 from interstitial chromosomal sequences. Intriguingly, TARs cover a much larger proportion of small chromosomes. We propose that this spatial bias increases relative DSB activity on smaller chromosomes and at least in part explains the increased recombination rate of small chromosomes.

METHODS

Yeast strains and synchronous meiosis

All strains used in this study are in the SK1 background and listed in **Table S1**.

Synchronous meiosis time-courses were performed as described in (Subramanian et al., 2016). The strains were first patched on glycerol media (YPG) and then transferred to rich media with 4% dextrose (YPD 4%). The cells were then grown at 23°C for 24 hrs in liquid YPD and diluted into pre-sporulation media (BYTA) at A_{600} 0.3. The BYTA culture was grown at 30°C for 16 hrs. The cells were washed twice in sterile water and transferred to sporulation media (0.3% potassium acetate) at 30°C to induce synchronous sporulation. Samples for ChIP-seq (25 mL) or DSB Southern assays (10mL) were collected at the indicated time-points.

DSB southern analysis

Meiotic cells collected at the indicated time points were embedded in agarose plugs to minimize background from random shearing and genomic DNA was extracted (Vader et al., 2011). The plugs were washed 4x 1hr in TE followed by 4x 1hr washes in the appropriate NEB buffer. Plugs for each time-point were transferred to separate tubes and melted at 65°C. The genomic DNA in molten agarose was equilibrated at 42°C prior to incubation with appropriate restriction

enzyme(s). The digested DNA was electrophoresed in 0.8% agarose (Seakem LE) in 1XTBE at 80V for 18 hrs. The DNA was transferred to Hybond-XL nylon membrane (GE Healthcare) by capillary transfer and detected by Southern hybridization as described in (Subramanian et al., 2016). Restriction enzymes used for DSB analysis and primer sequences to construct probes are listed in **Table S2**. Probes labeled with ^{32}P dCTP were generated using the listed primers and a Prime-It random labeling kit (Agilent). Southern blot was exposed to Fuji imaging screen and the phosphor-signal was detected on Typhoon FLA 9000 (GE) and quantified using ImageJ software (http://imagej.nih.gov/ij/). Plots were generated using the Graphpad program in Prism.

Chromatin immunoprecipitation and Illumina sequencing

Samples were collected from sporulation cultures at the indicated time points and crosslinked in 1% formaldehyde (Sigma) for 30 min. The formaldehyde was quenched with 125mM glycine. ChIP was performed as described in (Blitzblau et al., 2012) using antibodies listed in **Table S3**. Libraries for ChIP sequencing were prepared by PCR amplification with TruSeq adaptors (Illumina) as described in (Sun et al., 2015). Quality of the libraries was checked on 2100 Bioanalyzer or 2200 Tapestation. Libraries were quantified using qPCR prior to pooling. The ChIP libraries were sequenced on Illumina HiSeq 2500 or NextSeq 500 instruments at NYU Biology Genomics core to yield 50 bp single-end reads.

Processing of reads from Illumina sequencing

Illumina output reads were processed as described in (Paul et al., 2017). The reads were mapped to SK1 genome (Yue et al., 2017) using Bowtie (Langmead et al., 2009). Only reads that mapped to a single position and also matched perfectly to the SK1 genome were retrieved for further analysis. 3' ends of the reads were extended to a final length of 200bp using MACS2 2.1.1 (https://github.com/taoliu/MACS) and probabilistically determined PCR duplicates were removed. The input and ChIP pileups were SPMR-normalized (signal per million reads) and fold-enrichment of ChIP over input data was used for further analyses. The scripts used to process Illumina reads can be found at (https://github.com/hochwagenlab/ChIPseq_functions/tree/master/ChIPseq_Pipeline_v3/).

Quantitation of regional enrichment and statistical analyses

Average of two biological replicates was used for analyses. Averaged ChIP-seq data was normalized to global mean of one and regional enrichment was calculated, the scripts can be found at (https://github.com/hochwagenlab/hwglabr2/).

Mann-Whitney-Wilcox test or *t*-test was performed in R 3.3.3 to measure statistical significance. ANOVA for multiple linear regressions with interaction was performed on log2-scaled ChIP-seq enrichment to test variation in the slopes (chromosome size bias) of two different samples. For bootstrap analyses, 5000 random samplings of the ChIP data were performed. The samplings were equivalent to the experimental query in size and number for each experiment. The median and two-sided 95% CI was calculated based on the spread of the bootstrap-derived distribution of enrichment. To assay enrichment at the rDNA borders, TARs (120 Kb from either telomere) were excluded from the genome to obtain the random bootstrap-derived distribution.

Genome-wide DSB and resection datasets

Genome-wide DSB resection dataset for wild-type meiosis, Gene Expression Omnibus (GEO) accession number GSE85253, was obtained from (Mimitou et al., 2017). The processed dataset aligned to S288c reference genome (sacCer2) was used. The mapped Spo11-oligo counts for wild type and *zip3*Δ mutant, GEO number GSE48299, aligned to the S288c reference genome (sacCer2) were obtained from (Thacker et al., 2014). Additional wild-type Spo11-oligo counts data, GEO number GSE71930, also aligned to S288c reference genome (sacCer2) were obtained from (Lam and Keeney, 2015).

RESULTS

Continued DSB formation is linked to chromosomal position

To identify features that distinguish short- and long-lived hotspots, we expanded the number of hotspots whose lifespan has been classified using Southern assays. To exclude dampening of DSB activity because of prophase exit, we deleted the *NDT80* gene, which encodes a transcription factor necessary for initiating the prophase exit program (Chu and Herskowitz, 1998). *ndt80Δ* mutants halt meiotic progression at late prophase with fully synapsed chromosomes (pachynema) (Xu et al., 1995). Southern analysis of *ndt80Δ* cells undergoing a synchronous meiotic time course revealed new examples of short-lived (*YER004W*, *YER024W*, *YOR001W*) and long-lived hotspots (*YIL081W*, *YFL021W*) (**Figure 1A**, data not shown), indicating that both hotspot classes are common in the yeast genome.

Plotting the positions of these and previously published hotspots analyzed in *ndt80Δ* mutants revealed that the differences in temporal regulation correlated closely with distance from

telomeres. Whereas short-lived hotspots were located interstitially on chromosomes, long-lived hotspots were primarily found in large domains adjacent to the telomeres (**Figure 1B**). These data suggest that continued hotspot activity is linked to chromosomal position.

To extend this analysis across the genome, we assessed markers of DSB formation by ChIP-seq assay. Histone H2A phosphorylated on serine 129 (pH2A) is a well-documented chromatin modification that is activated by DSB formation and spreads into an approximately 50 Kb region around DNA breaks (Shroff et al., 2004; Unal et al., 2004). Samples were collected from synchronous *ndt80Δ* cultures at time points corresponding to early prophase (T=3hrs) and late prophase (T=6hrs), followed by deep sequencing of the pH2A chromatin immunoprecipitate. These analyses showed that pH2A is distributed relatively evenly along the chromosomes in early prophase, with particular enrichment at meiotic axis sites but depletion at DSB hotspots (**Figures S1A-C**). By contrast, pH2A enrichment was strongly biased towards the ends of all 16 chromosomes in late prophase (**Figure 1C**). This enrichment was most pronounced within 20-110 Kb from telomeres. We refer to these domains as telomere-adjacent regions (TARs). Averaging across all TARs revealed that this spatial bias was also apparent in early prophase, albeit to a significantly lesser extent (**Figure 1D**). At both time points, pH2A enrichment in the TARs was above the 95% confidence interval (CI) of a bootstrap-derived distribution (**Figure 1E**).

pH2A enrichment near telomeres was largely dependent on DNA break enzyme Spo11, indicating that these regions experience enhanced meiotic DSB activity. Consistently, ChIP-seq analysis of Rad51, a ssDNA binding protein, also showed an enrichment of signal in domains adjacent to the telomeres in late prophase (**Figures S1D and S1E**). We note that pH2A enrichment persisted within 20 Kb from telomeres in *spo11Δ* mutants, in line with previous observations showing DSB-independent enrichment in these regions in mitotic cells (Kim et al., 2007; Szilard et al., 2010). These observations suggest that DSB activity in TARs is prolonged relative to genome average.

To assess if elevated DSB activity in TARs is also detectable in wild-type cells (*NDT80*), we analyzed publicly available genome-wide datasets measuring meiotic DSB resection (Mimitou et al., 2017). Resection counts measure unrepaired DNA ends and thus also report on DSB occurrence. Resection signal became significantly enriched in TARs over time compared to interstitial chromosomal sequences (**Figure 1F, S1F**), closely mirroring the temporal enrichment

of pH2A and Rad51 in these regions. Analysis of available datasets (Lam and Keeney, 2015; Thacker et al., 2014) further showed that enrichment in Spo11-oligos, a byproduct of DSB formation, is also significantly higher in TARs compared to telomere-distal regions in mid/late prophase (T=4hrs; **Figure 1G, S1G**). Together, these data indicate that hotspots located in TARs are partially refractory to DSB down-regulation in late prophase.

Domains of continued DSB formation correlate with enrichment of Hop1

We sought to identify regulators mediating the differential DSB activity in late prophase. DSB activity depends on Hop1 and correlates well with the presence of Hop1 on chromosome spreads and in genome-wide assays (Borner et al., 2008; Panizza et al., 2011; Subramanian et al., 2016; Sun et al., 2015). Therefore, we monitored the evolution of Hop1 enrichment on wild-type (*NDT80*) meiotic chromosomes by ChIP-seq (**Figure S2**). At the time of pre-meiotic DNA replication (T=2hrs), Hop1 was enriched in large domains (~100 Kb) around the centromeres (>95% CI; **Figures S2A, S2D-E**). By early prophase (T=3hrs), Hop1 enrichment became more distributed and formed peaks of enrichment along all chromosomes (**Figure S2B**), matching previously defined sites of enrichment (Sun et al., 2015). Importantly, by mid/late prophase (T=4hrs), Hop1 enrichment trended significantly towards the TARs (**Figures S2C, S2F, S2G**). The increase of Hop1 enrichment in TARs was even more prominent in *ndt80Δ*-arrested late prophase cells (T=6hrs; **Figures 2A and B**). In both wild type and *ndt80Δ* mutants, the increase in Hop1 enrichment was above 95% CI for a bootstrap-derived distribution of enrichment along the genome (**Figure 2C**). These data suggest that continued DSB formation in the TARs is the result of persistent Hop1 enrichment in these domains.

To test if the redistribution of Hop1 in late prophase reflects an overall reorganization of the meiotic chromosome axis, we analyzed enrichment of the chromosome axis factor Red1 by ChIP-seq. Similar to Hop1, Red1 enrichment in TARs became more prominent in late prophase (**Figures 2D and 2E**). Red1 enrichment in TARs was above 95% CI compared to a bootstrap-derived enrichment along the genome (**Figure 2F**) and significantly different from enrichment at telomere-distal regions (**Figure 2D**, inset). The enhanced enrichment of axis proteins in the TARs suggests that meiotic chromatin remains poised for DSB formation in these regions during late prophase.

Because Hop1 recruits Mek1 kinase to meiotic chromosomes in response to DSB-induced checkpoint activation (Carballo et al., 2008; Niu et al., 2005), we also assessed Mek1

enrichment along chromosomes by ChIP-seq analysis in *ndt80Δ* cells (**Figures S3A and S3B**). Mek1 was enriched along the chromosomes in early prophase with specific enrichment at sites of axis protein binding and DSB hotspots (**Figures S3C, S3E**) (Pan et al., 2011; Sun et al., 2015), as well centromeres and tRNA genes (**Figures S3G and S3H**). Whereas Mek1 enrichment at axis sites persisted into late prophase, enrichment at hotspots was somewhat diminished likely reflecting a global reduction in DNA breakage in late prophase (**Figures S3D and S3F**). Importantly, Mek1 was significantly enhanced in the TARs in late prophase (**Figures 2F, 2G and S2B**, inset), providing further support that DSBs continue to form in these domains.

TAR-like regions flanking the ribosomal DNA

In addition to the TARs, Hop1 enrichment in late prophase also increased in ~100 Kb regions flanking the large ribosomal DNA (rDNA) array on chromosome XII (**Figure 3A**). This increase in enrichment was above the 95% CI of a bootstrap-derived distribution of enrichment in the genome (**Figure 3A**). A similar trend, albeit below the 95% CI, was observed in wild type (*NDT80*) cultures. Similar to TARs, the rDNA-adjacent Hop1 enrichment was accompanied by a significant local increase in pH2A signals (**Figure 3B**). Mek1 enrichment followed a similar trend but was below the 95% CI. To test if this enrichment reflected continued breakage of DNA in regions surrounding the rDNA, we measured DSB activity at the rDNA-adjacent *YLR152C* locus using Southern analysis. Time-course analysis in an *ndt80Δ* background revealed that DSBs and repair intermediates increase throughout the time course (**Figure 3C**), similar to long-lived hotspots in TARs (**Figure 1A**). These findings demonstrate ongoing DSB activity in late prophase next to the rDNA and suggest that the rDNA-adjacent regions, like TARs, escape negative feedback regulation of DSBs.

The SC protein Zip1 is equally present in TARs and interstitial regions

The Hop1 enrichment profile suggests that regulation of Hop1 in prophase is one predictor for the spatio-temporal regulation of DSB formation. Because cytological assays indicate that Hop1 is depleted from meiotic chromosomes upon SC assembly (Borner et al., 2008; San-Segundo and Roeder, 1999; Smith and Roeder, 1997; Subramanian et al., 2016), we asked if TARs are less likely to assemble an SC than interstitial chromosomal sequences. To test this model we surveyed localization of the SC central-region protein Zip1 on meiotic chromosomes by ChIP-seq. Consistent with previous reports, Zip1 was enriched around the centromeres (**Figure S4**). However, TAR enrichment of Zip1 in late prophase was not different from interstitial regions (*P*

= 0.564; **Figure 4**). These findings suggest that Zip1 assembly on chromosomes is not sufficient for the spatial regulation of Hop1 in late prophase.

Pch2 is required for late prophase enrichment profile of Hop1

The AAA^+-ATPase Pch2 is recruited to meiotic chromosomes upon SC assembly and is responsible for removal of Hop1 from the chromosomes (Borner et al., 2008; San-Segundo and Roeder, 1999; Subramanian et al., 2016). To test if Pch2 is responsible for establishing Hop1-enriched TARs in late prophase, we determined Hop1 binding in synchronous *pch2Δ ndt80Δ* cultures by ChIP-seq. These analyses showed abundant binding of Hop1 along chromosomes into late prophase, consistent with the persistent cytological signal of Hop1 in *pch2Δ* mutants. Importantly, Hop1 was no longer significantly enriched in TARs in *pch2Δ* mutants. An absence of specific enrichment was already observed in early prophase (T=3hrs). In late prophase (T=6hrs), Hop1 became significantly under-enriched in TARs (**Figures 5A-5C)**. These findings suggest that preferential Pch2-mediated Hop1 removal from interstitial regions enhances the relative Hop1 enrichment in the TARs.

In addition to TARs, we noted several genomic landmarks that were particularly affected by the loss of *PCH2*. As previously reported, Hop1 enrichment in *pch2Δ* mutants was increased within ~50 kb of the rDNA array, resulting in elevated DSB levels in these regions (Vader et al., 2011). This effect was further enhanced in late prophase (**Figure S5B, S5C**). In addition, we found that Hop1 enrichment was also elevated in the immediate vicinity of centromeres in *pch2* mutants (**Figure 5D**). The centromeric increase was already detectable above the 95% CI in early prophase and became even more pronounced in late prophase (**Figure 5E**). Accordingly, Southern analysis of a centromeric DSB hotspot (*YOR001W*) revealed elevated and persistent DSB activity in *pch2Δ ndt80Δ* mutants in late prophase (**Figure 5F**). These data indicate that Pch2 is required to restrict Hop1-linked DSB activity around the rDNA and at centromeres.

Enrichment of Hop1 and DSB markers exhibit a size bias, favoring small chromosomes

The fact that TARs occupy a proportionally much larger fraction of small chromosomes, provides a possible mechanism for increasing relative DSB levels on small chromosomes. Indeed, plotting pH2A enrichment/Kb as a function of chromosome size revealed a distinct, *SPO11*-dependent over-enrichment of pH2A on small chromosomes in late prophase (**Figure 6A**). A similarly biased enrichment on small chromosomes was also observed for Hop1 and Mek1 (**Figure 6B, C**). Biased enrichment of both proteins was already detectable in early

prophase but increased further in late prophase (**Figure 6B, C**). Moreover, increasing enrichment of Hop1 on small chromosomes occurred during prophase regardless of whether *NDT80* was present (**Figure S6A**).

The early enrichment of Hop1 and Mek1 on small chromosomes may be driven by the underlying enrichment of Red1 protein, which recruits Hop1 to chromosomes (Smith and Roeder, 1997; Woltering et al., 2000) and also exhibits chromosome size bias for enrichment in early prophase (**Figure S6B**) (Sun et al., 2015). Supporting this model, the pattern of chromosome size bias between Red1 and Hop1 in early prophase was not significantly different (ANOVA, p=0.167). However, the Red1 chromosome size bias did not increase between early and late prophase (**Figure S6B**), indicating that the late prophase enrichment of Hop1 (and Mek1) on small chromosomes occurs by a different mechanism. In support of TARs being responsible for the late prophase enrichment of Hop1 on small chromosomes, calculating the mean Hop1 enrichment per chromosome while excluding TARs and the rDNA borders, significantly reduces the chromosome size bias in late prophase (**Figure S6C**).

If TARs are responsible for the biased enrichment of Hop1 on small chromosomes then this effect should be abrogated in *pch2*Δ mutants, which do not exhibit Hop1 enrichment in TARs. Indeed, whereas the pattern of Hop1 chromosome size bias was not significantly different between *pch2*Δ and *PCH2* samples in early prophase (*P* = 0.691) (data not shown), in late prophase all chromosomes in *pch2*Δ mutants had a similar Hop1 enrichment/Kb irrespective of chromosome size (**Figure 6D**). These observations indicate that Pch2 is responsible for maintaining the chromosome size bias in prophase.

DISCUSSION

Our findings reveal striking regional control of DSB activity during meiosis. DSB hotspots in large domains (~100 Kb) adjacent to telomeres (TARs) as well as regions bordering the rDNA locus continue to break well after the SC down-regulates hotspots in interstitial chromosomal regions. This positional regulation increases the break potential on small chromosomes in the course of prophase, providing an intuitive mechanism for promoting formation of the obligatory crossover on small chromosomes.

Role of the SC in down-regulating hotspot activity

We found that the dichotomy in hotspot activity is due to specific spatial enrichment of the DSB activator Hop1 in the TARs during pachynema. Although a tight spatial correlation is observed in both *S. cerevisiae* and mouse between the deposition of the SC protein Zip1/Sycp1 and the Pch2/Trip13-dependent removal of Hop1/Hormad (Borner et al., 2008; San-Segundo and Roeder, 1999; Subramanian et al., 2016; Wojtasz et al., 2009), our findings show that Zip1 deposition is not sufficient for Hop1 eviction from the TARs. This observation suggests that additional factors or structural changes within the SC are involved in controlling Hop1 removal from chromosomes. Indeed, in *C. elegans*, which also utilizes the SC to down-regulate DSB formation in a timely manner, CO designation is thought to lead to structural changes within the SC that prevent further DSB formation (Hayashi et al., 2010; Libuda et al., 2013; Nadarajan et al., 2017; Rog et al., 2017). Our data indicate that Hop1 in TARs is either protected from these removal mechanisms, perhaps through TAR-enriched interacting proteins or posttranslational modifications, or it may be allowed to reload specifically in the TARs in late prophase. Preferential loading of Hop1 in the TARs is supported by the observation that similarly sized regions of elevated DSB activity are also observed in *dmc1*Δ mutants, which are defective in SC assembly (Blitzblau et al., 2007). Regardless of the mechanism, these data imply fundamental differences in the functional architecture of chromosomes that distinguish TARs from interstitial chromosomal regions.

Establishment of TARs

In the context of the yeast genome, TARs are unusually large functional regions, spanning nearly 100kb, which corresponds to almost half of the smallest yeast chromosome. Although the highly consistent positioning of TARs implies a role for telomeres in setting up this architecture, it is unclear how such long-range effects could be established. Telomeres are sites of heterochromatin nucleation but silencing complexes do not spread more than 20kb, even under overexpression conditions (Renauld et al., 1993). By contrast, TARs extend more than 5 times that distance and span many transcriptionally active genes. Perhaps the scale of the TARs is a reflection of different nuclear environments. Telomeres are tethered to the nuclear envelope (NE) and assemble into clusters during meiotic prophase in many organisms (Scherthan, 2007). Thus, a conceivable model is that proximity to the NE and/or telomere clustering promotes Hop1/Red1 enrichment in the TARs. NE proximity could also explain why TAR-like regions are flanking the rDNA locus, which is similarly juxtaposed to the NE (Carmo-Fonseca et al., 2000). We note, however, that disruption of several telomeric regulators, including the tethering factor *ESC1*, the telomere-length regulator *TEL1*, or the silencing factor *SIR3* did not significantly

affect enrichment of Hop1 at the TARs (data not shown). Depletion of the telomere clustering factor *NDJ1* may cause slight effects (V.V.S., unpublished results), but interpretation of this result is complicated by the fact that loss of *NDJ1* also causes synapsis defects (Conrad et al., 1997). The absence of strong phenotypes in these mutants may indicate that TARs are maintained by redundant mechanisms. Alternatively, Hop1 enrichment in the TARs in late prophase may be mediated by *cis* elements or other chromosome structures.

Control of DSBs near centromeres

In addition to the broad changes in enrichment of Hop1 across chromosomes during meiotic prophase, we also observed unexpected dynamics of Hop1 around centromeres. Most notably, we found a strong centromeric enrichment of Hop1 in the earliest stages of prophase, before Hop1 has fully accumulated on chromosome arms. Centromeric Hop1 enrichment may similarly reflect nuclear architecture because prior to the tethering of telomeres to the NE, the centromeres are clustered at the spindle pole body embedded in the NE (Hayashi et al., 1998; Jin et al., 2000). Interestingly, the early prophase dynamics of Hop1 mirrors the distribution of Spo11, which is also enriched near centromeres before distributing to the arms (Kugou et al., 2009). Indeed, Spo11 is likely active in these regions because we observe centromeric DSBs in early prophase (Figure 5). Curiously, we also detected an enrichment of Mek1 around the centromeres. Recruitment of Mek1 is unexpected because Mek1 suppresses repair with the sister chromatid (Niu et al., 2005; Subramanian et al., 2016; Wu et al., 2010), yet DSBs at centromeres are thought to be channeled by Zip1 to primarily use the sister for recombination to protect against chromosome missegregation (Chen et al., 2008; Vincenten et al., 2015). Perhaps, in addition to mediating Mek1 removal from synapsed chromosomes (Subramanian et al., 2016), Zip1 also suppresses Mek1 activity at the centromeres without evicting it. Another unexpected finding is that Pch2 suppresses DSBs around centromeres in late prophase. However, as COs are not enhanced around the centromeres in *pch2*Δ mutants (Chakraborty et al., 2017), Zip1 activity must be sufficient to prevent any deleterious inter-homologue COs in this situation. These findings indicate that several mechanistic layers restrict DSBs and COs at the centromeres, highlighting the importance of limiting COs in this region.

TARs: an unbiased mechanism that contributes to bias

Our analysis of Hop1 dynamics sheds important light on the mechanistic basis of the meiotic chromosome-size bias for recombination. In several organisms, including humans, small chromosomes exhibit higher levels of recombination (Backstrom et al., 2010; Chakraborty et al.,

2017; Kaback, 1996; Kaback et al., 1992; Kaback et al., 1989; Lange et al., 2016), a bias that in yeast is already apparent from elevated levels of axis protein deposition and DSB formation on small chromosomes (Blitzblau et al., 2007; Gerton et al., 2000; Lam and Keeney, 2015; Pan et al., 2011; Thacker et al., 2014). As TAR length remains invariant regardless of chromosome size, TARs comprise a proportionally much larger fraction of small chromosomes (**Figure 7**). The resulting bias in Hop1 enrichment could thus partially mediate the establishment of chromosome size bias in DSBs and crossovers. Intriguingly, COs are enriched in sub-telomeric regions in several organisms (Auton et al., 2012; Backstrom et al., 2010; Barnes et al., 1995; Mohrenweiser et al., 1998; Rockman and Kruglyak, 2009; Singhal et al., 2015; Yu et al., 2001). Moreover, an ancient telomeric fusion that gave rise to human chromosome 2 led to a decrease in crossovers rates near the fused chromosome ends compared to chimpanzees, which maintained the two separate chromosomes (Auton et al., 2012). Thus, some fundamental features of TARs may well be evolutionarily conserved.

Available data suggests that chromosome size bias for Hop1 enrichment in late prophase is a direct consequence of preferential SC-dependent removal of Hop1 from the interstitial chromosomal regions. Consistent with this notion, disrupting either CO-associated SC assembly (by deleting the CO-designating factor *ZIP3*) or preventing the SC from removing Hop1 (by deleting *PCH2*) leads to a loss of chromosome size bias for recombination (Chakraborty et al., 2017; Thacker et al., 2014; Zanders et al., 2011). In both situations, the failure to remove Hop1 has a differential effect on the TARs. DSB enrichment in TARs is diminished in *zip3*Δ mutants compared to wild type (P = 0.58, Mann-Whitney-Wilcox test; **Figure S6D**). Similarly, the percentage of COs and noncrossovers per meiosis was found to drop significantly in the TARs of *pch2*Δ mutants compared to wild type spores, while average CO (and non-CO) counts per chromosome surge with increasing chromosome size in this mutant (Chakraborty et al., 2017).

We propose that TARs provide a safety mechanism that ensures that DSB formation is not prematurely inactivated by the formation of the SC. Premature down-regulation of the DSB machinery is particularly problematic for small chromosomes because of their inherently smaller number of DSB hotspots. By establishing privileged regions that are refractory to this down-regulation, cells may ensure that all chromosomes retain a (limited) potential for DSB formation and successful crossover recombination throughout meiotic prophase.

ACKNOWLEDGEMENTS

We are grateful to Brian Parker at NYU for advice on statistics. We thank the NYU Genomics Core facility for technical assistance and data processing. This work was funded in part by grant R01 GM111715 from the NIH and research grant #6-FY16-208 from the March of Dimes Foundation to A.H.

REFERENCES

Allers, T., and Lichten, M. (2001). Differential timing and control of noncrossover and crossover recombination during meiosis. Cell *106*, 47-57.

Auton, A., Fledel-Alon, A., Pfeifer, S., Venn, O., Segurel, L., Street, T., Leffler, E.M., Bowden, R., Aneas, I., Broxholme, J.*, et al.* (2012). A fine-scale chimpanzee genetic map from population sequencing. Science *336*, 193-198.

Backstrom, N., Forstmeier, W., Schielzeth, H., Mellenius, H., Nam, K., Bolund, E., Webster, M.T., Ost, T., Schneider, M., Kempenaers, B.*, et al.* (2010). The recombination landscape of the zebra finch *Taeniopygia guttata* genome. Genome Research *20*, 485-495.

Barnes, T.M., Kohara, Y., Coulson, A., and Hekimi, S. (1995). Meiotic recombination, noncoding DNA and genomic organization in *Caenorhabditis elegans*. Genetics *141*, 159-179.

Baudat, F., and Nicolas, A. (1997). Clustering of meiotic double-strand breaks on yeast chromosome III. Proceedings of the National Academy of Sciences *94*, 5213-5218.

Bickel, S.E., Orr-Weaver, T.L., and Balicky, E.M. (2002). The sister-chromatid cohesion protein ORD is required for chiasma maintenance in Drosophila oocytes. Current Biology *12*, 925-929.

Blat, Y., Protacio, R.U., Hunter, N., and Kleckner, N. (2002). Physical and functional interactions among basic chromosome organizational features govern early steps of meiotic chiasma formation. Cell *111*, 791-802.

Blitzblau, H.G., Bell, G.W., Rodriguez, J., Bell, S.P., and Hochwagen, A. (2007). Mapping of meiotic single-stranded DNA reveals double-stranded-break hotspots near centromeres and telomeres. Current Biology *17*, 2003-2012.

Blitzblau, H.G., Chan, C.S., Hochwagen, A., and Bell, S.P. (2012). Separation of DNA replication from the assembly of break-competent meiotic chromosomes. PLoS Genetics *8*, e1002643.

Blitzblau, H.G., and Hochwagen, A. (2013). ATR/Mec1 prevents lethal meiotic recombination initiation on partially replicated chromosomes in budding yeast. eLife *2*, e00844.

Borde, V., and de Massy, B. (2013). Programmed induction of DNA double strand breaks during meiosis: setting up communication between DNA and the chromosome structure. Current Opinion in Genetics & Development *23*, 147-155.

Borner, G.V., Barot, A., and Kleckner, N. (2008). Yeast Pch2 promotes domainal axis organization, timely recombination progression, and arrest of defective recombinosomes during meiosis. Proceedings of the National Academy of Sciences *105*, 3327-3332.

Buhler, C., Borde, V., and Lichten, M. (2007). Mapping meiotic single-strand DNA reveals a new landscape of DNA double-strand breaks in *Saccharomyces cerevisiae*. PLoS Biology *5*, e324.

Buonomo, S.B., Clyne, R.K., Fuchs, J., Loidl, J., Uhlmann, F., and Nasmyth, K. (2000). Disjunction of homologous chromosomes in meiosis I depends on proteolytic cleavage of the meiotic cohesin Rec8 by separin. Cell *103*, 387-398.

Carballo, J.A., Johnson, A.L., Sedgwick, S.G., and Cha, R.S. (2008). Phosphorylation of the axial element protein Hop1 by Mec1/Tel1 ensures meiotic interhomolog recombination. Cell *132*, 758-770.

Carmo-Fonseca, M., Mendes-Soares, L., and Campos, I. (2000). To be or not to be in the nucleolus. Nature Cell Biology *2*, E107-112.

Chakraborty, P., Pankajam, A.V., Lin, G., Dutta, A., Krishnaprasad, G.N., Tekkedil, M.M., Shinohara, A., Steinmetz, L.M., and Nishant, K.T. (2017). Modulating Crossover Frequency and Interference for Obligate Crossovers in *Saccharomyces cerevisiae* Meiosis. G3 *7*, 1511-1524.

Chen, S.Y., Tsubouchi, T., Rockmill, B., Sandler, J.S., Richards, D.R., Vader, G., Hochwagen, A., Roeder, G.S., and Fung, J.C. (2008). Global analysis of the meiotic crossover landscape. Developmental Cell *15*, 401-415.

Chu, S., and Herskowitz, I. (1998). Gametogenesis in yeast is regulated by a transcriptional cascade dependent on Ndt80. Molecular cell *1*, 685-696.

Conrad, M.N., Dominguez, A.M., and Dresser, M.E. (1997). Ndj1p, a meiotic telomere protein required for normal chromosome synapsis and segregation in yeast. Science *276*, 1252-1255.

Cooper, T.J., Garcia, V., and Neale, M.J. (2016). Meiotic DSB patterning: A multifaceted process. Cell cycle *15*, 13-21.

de Massy, B. (2013). Initiation of meiotic recombination: how and where? Conservation and specificities among eukaryotes. Annual review of genetics *47*, 563-599.

Fung, J.C., Rockmill, B., Odell, M., and Roeder, G.S. (2004). Imposition of crossover interference through the nonrandom distribution of synapsis initiation complexes. Cell *116*, 795-802.

Garcia, V., Gray, S., Allison, R.M., Cooper, T.J., and Neale, M.J. (2015). Tel1(ATM)-mediated interference suppresses clustered meiotic double-strand-break formation. Nature *520*, 114-118.

Gerton, J.L., DeRisi, J., Shroff, R., Lichten, M., Brown, P.O., and Petes, T.D. (2000). Global mapping of meiotic recombination hotspots and coldspots in the yeast Saccharomyces cerevisiae. Proceedings of the National Academy of Sciences *97*, 11383-11390.

Goodyer, W., Kaitna, S., Couteau, F., Ward, J.D., Boulton, S.J., and Zetka, M. (2008). HTP-3 links DSB formation with homolog pairing and crossing over during *C. elegans* meiosis. Developmental Cell *14*, 263-274.

Gray, S., Allison, R.M., Garcia, V., Goldman, A.S., and Neale, M.J. (2013). Positive regulation of meiotic DNA double-strand break formation by activation of the DNA damage checkpoint kinase Mec1(ATR). Open Biology *3*, 130019.

Gray, S., and Cohen, P.E. (2016). Control of Meiotic Crossovers: From Double-Strand Break Formation to Designation. Annual Review of Genetics *50*, 175-210.

Hayashi, A., Ogawa, H., Kohno, K., Gasser, S.M., and Hiraoka, Y. (1998). Meiotic behaviours of chromosomes and microtubules in budding yeast: relocalization of centromeres and telomeres during meiotic prophase. Genes to Cells *3*, 587-601.

Hayashi, M., Mlynarczyk-Evans, S., and Villeneuve, A.M. (2010). The synaptonemal complex shapes the crossover landscape through cooperative assembly, crossover promotion and crossover inhibition during *Caenorhabditis elegans* meiosis. Genetics *186*, 45-58.

Hunter, N. (2015). Meiotic Recombination: The Essence of Heredity. Cold Spring Harbor Perspectives in Biology *7*.

Jin, Q.W., Fuchs, J., and Loidl, J. (2000). Centromere clustering is a major determinant of yeast interphase nuclear organization. Journal of Cell Science *113 (Pt 11)*, 1903-1912.

Kaback, D.B. (1996). Chromosome-size dependent control of meiotic recombination in humans. Nature genetics *13*, 20-21.

Kaback, D.B., Guacci, V., Barber, D., and Mahon, J.W. (1992). Chromosome size-dependent control of meiotic recombination. Science *256*, 228-232.

Kaback, D.B., Steensma, H.Y., and de Jonge, P. (1989). Enhanced meiotic recombination on the smallest chromosome of *Saccharomyces cerevisiae*. Proceedings of the National Academy of Sciences *86*, 3694-3698.

Kim, J.A., Kruhlak, M., Dotiwala, F., Nussenzweig, A., and Haber, J.E. (2007). Heterochromatin is refractory to gamma-H2AX modification in yeast and mammals. The Journal of Cell Biology *178*, 209-218.

Kim, K.P., Weiner, B.M., Zhang, L., Jordan, A., Dekker, J., and Kleckner, N. (2010). Sister cohesion and structural axis components mediate homolog bias of meiotic recombination. Cell *143*, 924-937.

Kim, Y., Rosenberg, S.C., Kugel, C.L., Kostow, N., Rog, O., Davydov, V., Su, T.Y., Dernburg, A.F., and Corbett, K.D. (2014). The chromosome axis controls meiotic events through a hierarchical assembly of HORMA domain proteins. Developmental Cell *31*, 487-502.

Kleckner, N. (1996). Meiosis: how could it work? Proceedings of the National Academy of Sciences *93*, 8167-8174.

Kudo, N.R., Wassmann, K., Anger, M., Schuh, M., Wirth, K.G., Xu, H., Helmhart, W., Kudo, H., McKay, M., Maro, B.*, et al.* (2006). Resolution of chiasmata in oocytes requires separase-mediated proteolysis. Cell *126*, 135-146.

Kugou, K., Fukuda, T., Yamada, S., Ito, M., Sasanuma, H., Mori, S., Katou, Y., Itoh, T., Matsumoto, K., Shibata, T.*, et al.* (2009). Rec8 guides canonical Spo11 distribution along yeast meiotic chromosomes. Molecular Biology of the Cell *20*, 3064-3076.

Kumar, R., Bourbon, H.M., and de Massy, B. (2010). Functional conservation of Mei4 for meiotic DNA double-strand break formation from yeasts to mice. Genes & Development *24*, 1266-1280.

Kumar, R., Ghyselinck, N., Ishiguro, K., Watanabe, Y., Kouznetsova, A., Hoog, C., Strong, E., Schimenti, J., Daniel, K., Toth, A.*, et al.* (2015). MEI4 - a central player in the regulation of meiotic DNA double-strand break formation in the mouse. Journal of Cell Science *128*, 1800-1811.

Lam, I., and Keeney, S. (2014). Mechanism and regulation of meiotic recombination initiation. Cold Spring Harbor Perspectives in Biology *7*, a016634.

Lam, I., and Keeney, S. (2015). Nonparadoxical evolutionary stability of the recombination initiation landscape in yeast. Science *350*, 932-937.

Lange, J., Yamada, S., Tischfield, S.E., Pan, J., Kim, S., Zhu, X., Socci, N.D., Jasin, M., and Keeney, S. (2016). The Landscape of Mouse Meiotic Double-Strand Break Formation, Processing, and Repair. Cell *167*, 695-708 e616.

Langmead, B., Trapnell, C., Pop, M., and Salzberg, S.L. (2009). Ultrafast and memory-efficient alignment of short DNA sequences to the human genome. Genome Biology *10*, R25.

Lee, J.Y., and Orr-Weaver, T.L. (2001). The molecular basis of sister-chromatid cohesion. Annual Review of Cell and Developmental Biology *17*, 753-777.

Libuda, D.E., Uzawa, S., Meyer, B.J., and Villeneuve, A.M. (2013). Meiotic chromosome structures constrain and respond to designation of crossover sites. Nature. *502*, 703-706.

Mao-Draayer, Y., Galbraith, A.M., Pittman, D.L., Cool, M., and Malone, R.E. (1996). Analysis of meiotic recombination pathways in the yeast Saccharomyces cerevisiae. Genetics *144*, 71-86.

Mehrotra, S., and McKim, K.S. (2006). Temporal analysis of meiotic DNA double-strand break formation and repair in Drosophila females. PLoS Genetics *2*, e200.

Mets, D.G., and Meyer, B.J. (2009). Condensins regulate meiotic DNA break distribution, thus crossover frequency, by controlling chromosome structure. Cell *139*, 73-86.

Mimitou, E.P., Yamada, S., and Keeney, S. (2017). A global view of meiotic double-strand break end resection. Science *355*, 40-45.

Miyoshi, T., Ito, M., Kugou, K., Yamada, S., Furuichi, M., Oda, A., Yamada, T., Hirota, K., Masai, H., and Ohta, K. (2012). A central coupler for recombination initiation linking chromosome architecture to S phase checkpoint. Molecular Cell *47*, 722-733.

Mohrenweiser, H.W., Tsujimoto, S., Gordon, L., and Olsen, A.S. (1998). Regions of sex-specific hypo- and hyper-recombination identified through integration of 180 genetic markers into the metric physical map of human chromosome 19. Genomics *47*, 153-162.

Moore, D.P., and Orr-Weaver, T.L. (1998). Chromosome segregation during meiosis: building an unambivalent bivalent. Current Topics in Developmental Biology *37*, 263-299.

Murakami, H., and Keeney, S. (2014). Temporospatial coordination of meiotic DNA replication and recombination via DDK recruitment to replisomes. Cell *158*, 861-873.

Nadarajan, S., Lambert, T.J., Altendorfer, E., Gao, J., Blower, M.D., Waters, J.C., and Colaiacovo, M.P. (2017). Polo-like kinase-dependent phosphorylation of the synaptonemal complex protein SYP-4 regulates double-strand break formation through a negative feedback loop. eLife *6*.

Niu, H., Wan, L., Baumgartner, B., Schaefer, D., Loidl, J., and Hollingsworth, N.M. (2005). Partner choice during meiosis is regulated by Hop1-promoted dimerization of Mek1. Molecular biology of the cell *16*, 5804-5818.

Ogino, K., and Masai, H. (2006). Rad3-Cds1 mediates coupling of initiation of meiotic recombination with DNA replication. Mei4-dependent transcription as a potential target of meiotic checkpoint. The Journal of Biological Chemistry *281*, 1338-1344.

Page, S.L., and Hawley, R.S. (2003). Chromosome choreography: the meiotic ballet. Science *301*, 785-789.

Pan, J., Sasaki, M., Kniewel, R., Murakami, H., Blitzblau, H.G., Tischfield, S.E., Zhu, X., Neale, M.J., Jasin, M., Socci, N.D.*, et al.* (2011). A hierarchical combination of factors shapes the genome-wide topography of yeast meiotic recombination initiation. Cell *144*, 719-731.

Panizza, S., Mendoza, M.A., Berlinger, M., Huang, L., Nicolas, A., Shirahige, K., and Klein, F. (2011). Spo11-accessory proteins link double-strand break sites to the chromosome axis in early meiotic recombination. Cell *146*, 372-383.

Paul, M.R., Markowitz, T.E., Hochwagen, A., and Ercan, S. (2017). Acute condensin depletion causes genome decompaction without altering the level of global gene expression in Saccharomyces cerevisiae. bioRxiv.

Petronczki, M., Siomos, M.F., and Nasmyth, K. (2003). Un menage a quatre: the molecular biology of chromosome segregation in meiosis. Cell *112*, 423-440.

Renauld, H., Aparicio, O.M., Zierath, P.D., Billington, B.L., Chhablani, S.K., and Gottschling, D.E. (1993). Silent domains are assembled continuously from the telomere and are defined by promoter distance and strength, and by *SIR3* dosage. Genes & Development *7*, 1133-1145.

Rockman, M.V., and Kruglyak, L. (2009). Recombinational landscape and population genomics of Caenorhabditis elegans. PLoS Genetics *5*, e1000419.

Rog, O., Kohler, S., and Dernburg, A.F. (2017). The synaptonemal complex has liquid crystalline properties and spatially regulates meiotic recombination factors. eLife *6*.

San-Segundo, P.A., and Roeder, G.S. (1999). Pch2 links chromatin silencing to meiotic checkpoint control. Cell *97*, 313-324.

Scherthan, H. (2007). Telomere attachment and clustering during meiosis. Cellular and Molecular Life Sciences : CMLS *64*, 117-124.

Serrentino, M.E., Chaplais, E., Sommermeyer, V., and Borde, V. (2013). Differential association of the conserved SUMO ligase Zip3 with meiotic double-strand break sites reveals regional variations in the outcome of meiotic recombination. PLoS Genetics *9*, e1003416.

Shroff, R., Arbel-Eden, A., Pilch, D., Ira, G., Bonner, W.M., Petrini, J.H., Haber, J.E., and Lichten, M. (2004). Distribution and dynamics of chromatin modification induced by a defined DNA double-strand break. Current biology *14*, 1703-1711.

Singhal, S., Leffler, E.M., Sannareddy, K., Turner, I., Venn, O., Hooper, D.M., Strand, A.I., Li, Q., Raney, B., Balakrishnan, C.N.*, et al.* (2015). Stable recombination hotspots in birds. Science *350*, 928-932.

Smith, A.V., and Roeder, G.S. (1997). The yeast Red1 protein localizes to the cores of meiotic chromosomes. The Journal of Cell Biology *136*, 957-967.

Sommermeyer, V., Beneut, C., Chaplais, E., Serrentino, M.E., and Borde, V. (2013). Spp1, a member of the Set1 Complex, promotes meiotic DSB formation in promoters by tethering histone H3K4 methylation sites to chromosome axes. Molecular Cell *49*, 43-54.

Subramanian, V.V., and Hochwagen, A. (2014). The meiotic checkpoint network: step-by-step through meiotic prophase. Cold Spring Harbor Perspectives in Biology *6*, a016675.

Subramanian, V.V., MacQueen, A.J., Vader, G., Shinohara, M., Sanchez, A., Borde, V., Shinohara, A., and Hochwagen, A. (2016). Chromosome Synapsis Alleviates Mek1-Dependent Suppression of Meiotic DNA Repair. PLoS Biology *14* e1002369.

Sun, X., Huang, L., Markowitz, T.E., Blitzblau, H.G., Chen, D., Klein, F., and Hochwagen, A. (2015). Transcription dynamically patterns the meiotic chromosome-axis interface. eLife *4*.

Szilard, R.K., Jacques, P.E., Laramee, L., Cheng, B., Galicia, S., Bataille, A.R., Yeung, M., Mendez, M., Bergeron, M., Robert, F.*, et al.* (2010). Systematic identification of fragile sites via genome-wide location analysis of gamma-H2AX. Nature structural & molecular biology *17*, 299-305.

Thacker, D., Mohibullah, N., Zhu, X., and Keeney, S. (2014). Homologue engagement controls meiotic DNA break number and distribution. Nature *510*, 241-246.

Tonami, Y., Murakami, H., Shirahige, K., and Nakanishi, M. (2005). A checkpoint control linking meiotic S phase and recombination initiation in fission yeast. Proceedings of the National Academy of Sciences *102*, 5797-5801.

Unal, E., Arbel-Eden, A., Sattler, U., Shroff, R., Lichten, M., Haber, J.E., and Koshland, D. (2004). DNA damage response pathway uses histone modification to assemble a double-strand break-specific cohesin domain. Molecular Cell *16*, 991-1002.

Vader, G., Blitzblau, H.G., Tame, M.A., Falk, J.E., Curtin, L., and Hochwagen, A. (2011). Protection of repetitive DNA borders from self-induced meiotic instability. Nature *477*, 115-119.

van Heemst, D., and Heyting, C. (2000). Sister chromatid cohesion and recombination in meiosis. Chromosoma *109*, 10-26.

Vincenten, N., Kuhl, L.M., Lam, I., Oke, A., Kerr, A.R., Hochwagen, A., Fung, J., Keeney, S., Vader, G., and Marston, A.L. (2015). The kinetochore prevents centromere-proximal crossover recombination during meiosis. eLife *4*.

Wojtasz, L., Daniel, K., Roig, I., Bolcun-Filas, E., Xu, H., Boonsanay, V., Eckmann, C.R., Cooke, H.J., Jasin, M., Keeney, S.*, et al.* (2009). Mouse HORMAD1 and HORMAD2, two conserved meiotic chromosomal proteins, are depleted from synapsed chromosome axes with the help of TRIP13 AAA-ATPase. PLoS Genetics *5*, e1000702.

Woltering, D., Baumgartner, B., Bagchi, S., Larkin, B., Loidl, J., de los Santos, T., and Hollingsworth, N.M. (2000). Meiotic segregation, synapsis, and recombination checkpoint functions require physical interaction between the chromosomal proteins Red1p and Hop1p. Molecular and Cellular Biology *20*, 6646-6658.

Wu, H.Y., Ho, H.C., and Burgess, S.M. (2010). Mek1 kinase governs outcomes of meiotic recombination and the checkpoint response. Current biology *20*, 1707-1716.

Xu, L., Ajimura, M., Padmore, R., Klein, C., and Kleckner, N. (1995). NDT80, a meiosis-specific gene required for exit from pachytene in Saccharomyces cerevisiae. Molecular and Cellular Biology *15*, 6572-6581.

Xu, L., Weiner, B.M., and Kleckner, N. (1997). Meiotic cells monitor the status of the interhomolog recombination complex. Genes & Development *11*, 106-118.

Yu, A., Zhao, C., Fan, Y., Jang, W., Mungall, A.J., Deloukas, P., Olsen, A., Doggett, N.A., Ghebranious, N., Broman, K.W.*, et al.* (2001). Comparison of human genetic and sequence-based physical maps. Nature *409*, 951-953.

Yu, Z., Kim, Y., and Dernburg, A.F. (2016). Meiotic recombination and the crossover assurance checkpoint in *Caenorhabditis elegans*. Seminars in Cell & Developmental Biology *54*, 106-116.

Yue, J.X., Li, J., Aigrain, L., Hallin, J., Persson, K., Oliver, K., Bergstrom, A., Coupland, P., Warringer, J., Lagomarsino, M.C.*, et al.* (2017). Contrasting evolutionary genome dynamics between domesticated and wild yeasts. Nature Genetics *49*, 913-924.

Zanders, S., Sonntag Brown, M., Chen, C., and Alani, E. (2011). Pch2 modulates chromatid partner choice during meiotic double-strand break repair in *Saccharomyces cerevisiae*. Genetics *188*, 511-521.

Zhang, L., Kim, K.P., Kleckner, N.E., and Storlazzi, A. (2011). Meiotic double-strand breaks occur once per pair of (sister) chromatids and, via Mec1/ATR and Tel1/ATM, once per quartet of chromatids. Proceedings of the National Academy of Sciences *108*, 20036-20041.

FIGURE LEGENDS

Figure1

Long-lived DSB hotspots occur primarily in TARs.

(A) Southern analysis to monitor DSBs from *ndt80Δ* cells progressing synchronously though meiotic prophase at *YOL081W* (a long-lived DSB hotspot, orange outline) and *YER024W* (a short-lived DSB hotspot, magenta outline). Black arrow points to continued DSBs in late prophase (6hrs) at the *YOL081W* DSB hotspot. * nonspecific bands. (B) Distance of a few queried DSB hotspots (orange, long-lived; magenta, short-lived) from their closest telomere ((Allers and Lichten, 2001; Subramanian et al., 2016; Xu et al., 1995); this manuscript, and data not shown). (C) pH2A ChIP-seq enrichment is plotted along each of the 16 yeast chromosomes, black triangles mark the centromeres. The data are normalized to a global mean of 1. Inset shows mean enrichment at TARs (20-110 Kb from telomeres; orange) and interstitial chromosomal regions (>110 Kb from telomeres; magenta) in early prophase (T=3hrs) and late prophase (T=6hrs). *** $P < 0.001$, Mann-Whitney-Wilcoxon test. (D) pH2A enrichment plotted as a mean enrichment of the 32 chromosome ends as a function of distance from telomeres. The dotted light grey line depicts genome average. (E) Bootstrap-derived distributions from ChIP-seq data are shown as violin plots. Lower and upper quantile (95% confidence intervals, CI) as well as the median computed from the bootstrap data are depicted as horizontal lines. The red dot shows the mean ChIP-seq enrichment at TARs (20-110 Kb) for the respective samples. The grey dotted line is the genome average. (F) Time series of resected DSB ends (Mimitou et al., 2017) are normalized to genome average and plotted as mean signal in TARs (20-110 Kb, 32 domains) and interstitial chromosomal regions (>110 Kb from either end of all chromosomes, 16 domains). The grey dotted line is the genome average. ** $P < 0.01$ and * $P < 0.05$, *t*-test of means. (G) Spo11-oligo levels (Lam and Keeney, 2015; Thacker et al., 2014) are normalized to genome average and plotted as mean signal in TARs (20-110 Kb, 32 domains) and interstitial chromosomal regions (>110 Kb from either end of all chromosomes, 16 domains). The grey dotted line is the genome average. ** $P < 0.01$ and * $P < 0.05$, *t*-test of means.

Figure2

Chromosomal proteins upstream and downstream of DSB formation become enriched in TARs during prophase.

(A) Hop1 ChIP-seq enrichment (dark green) in *ndt80Δ*-arrested late prophase cells plotted along each of the 16 yeast chromosomes, black triangles mark the centromeres. The data are normalized to a global mean of 1. Inset shows mean enrichment in TARs (20-110 Kb, orange) and interstitial chromosomal regions (magenta) in early prophase (T=3hrs) and late prophase (T=6hrs). *** $P < 0.001$, Mann-Whitney-Wilcoxon test. (B) Hop1 enrichment plotted as a mean of the 32 chromosome ends as a function of distance from telomeres. The grey dotted line is genome average. (C) Bootstrap-derived distributions from ChIP-seq data depicted as violin plots. Additionally, the horizontal lines in the violin plots represent the median and the two-ended CIs. The mean Hop1 ChIP-seq enrichment in TARs (20-110 Kb) for the respective samples is shown as red dots. (D) Red1 ChIP-seq enrichment (dark red) in *ndt80Δ*-arrested late prophase cells plotted along each of the 16 yeast chromosomes, black triangles mark the centromeres. The data are normalized to a global mean of one. Inset shows mean enrichment in TARs (20-110 Kb, orange) and interstitial chromosomal regions (magenta) in early prophase (T=3hrs) and late prophase (T=6hrs). *** $P < 0.001$ and ** $P < 0.01$, Mann-Whitney-Wilcoxon test. (E) Red1 enrichment plotted as a mean of the 32 chromosome ends as a function of distance from telomeres. The grey dotted line is genome average. (F) Bootstrap-derived distributions are shown as violin plots and the horizontal lines within the plots represent the median and the two-ended 95% CIs. The mean ChIP-seq enrichment at the TARs (20-110 Kb) for the respective samples is shown as black dots. (G) Mek1 enrichment plotted as a mean of the 32 chromosome ends as function of the distance from telomeres. The grey dotted line is genome average.

Figure3

rDNA-adjacent regions are enriched for Hop1 and long-lived DSBs in late prophase.

(A) Schematic of rDNA-adjacent regions (100 Kb on either side) enriched for Hop1 and DSB markers (upper panel). Lower panel: Bootstrap-derived distributions from Hop1 ChIP-seq data illustrated as violin plots. The horizontal lines in the violin plots represent the median and the two-ended CIs. The mean Hop1 ChIP-seq enrichment at rDNA-adjacent domains (100 Kb) for the respective samples is shown as red dots. (B) Bootstrap-derived distributions from pH2A and Mek1 ChIP-seq data shown as violin plots. The horizontal lines in the violin plots represent the median and the two-ended 95% CIs. The mean ChIP-seq enrichment at rDNA-adjacent domains (100 Kb) for the respective samples is shown as red dots. (C) Southern analysis to monitor DSBs and repair intermediates at *YLR152C* DSB hotspot adjacent to the rDNA (upper

panel). Lower panel: The percentage of DSB formation at the *YLR152C* locus over total DNA at the indicated time points. DSBs are plotted as the sum of DSBs and repair intermediates. The data are mean of three independent biological replicates and error bars represent standard deviation from the mean.

Figure4

Zip1 is not depleted from TARs.

(A) Zip1 ChIP-seq enrichment (magenta) in *ndt80Δ*-arrested late prophase cells plotted along each of the 16 yeast chromosomes, black triangles mark the centromeres. The data are normalized to a global mean of 1. Inset shows mean enrichment in TARs (20-110 Kb, orange) and interstitial chromosomal regions (magenta) in late prophase (T=6hrs). P = 0.564, Mann-Whitney-Wilcoxon test. (B) Hop1 (dark green) and Zip1 (magenta) ChIP-seq enrichment in late prophase (6hrs) is plotted as a mean of the 32 chromosome ends as a function of the distance from telomeres. The grey dotted line is genome average. (C) Bootstrap-derived distributions from Zip1 ChIP-seq data illustrated as a violin plot. The horizontal lines in the violin plots represent the median and the two-ended 95% CIs. The mean Zip1 ChIP-seq enrichment in TARs (20-110 Kb) is shown as a black dot.

Figure5

Pch2 controls regional distribution of Hop1 in late prophase.

(A) Hop1 ChIP-seq enrichment in *pch2Δ ndt80Δ* late prophase (6hrs) cells plotted along each of the 16 yeast chromosomes, black triangles mark the centromeres. The data are normalized to a global mean of 1. Inset shows mean Hop1 enrichment in TARs (20-110 Kb, orange) and interstitial chromosomal regions (magenta) in early prophase (T=3hrs) and late prophase (T=6hrs). ** $P < 0.01$ and * $P < 0.05$, Mann-Whitney-Wilcoxon test. (B) Mean Hop1 enrichment at chromosome ends normalized to genome average as a function of the distance from telomeres. The grey dotted line is genome average. (C) Bootstrap-derived distributions from ChIP-seq data illustrated as violin plots. The horizontal lines in the violin plots represent the median and the two-ended 95% CIs. The mean Hop1 ChIP-seq enrichment in TARs (20-110 Kb) for the respective samples is shown as black dots. The grey dotted line is genome average. (D) Mean Hop1 enrichment around the centromeres normalized to genome average as a function of the distance from centromeres. The grey dotted line is genome average. The grey

dotted line is genome average. (E) Bootstrap-derived distributions from ChIP-seq data illustrated as violin plots. The horizontal lines in the violin plots represent the median and the two-ended 95% CIs. The mean Hop1 ChIP-seq enrichment around centromeres (2 Kb) for the respective samples is shown as black dots. (F) Southern analysis to monitor DSBs at the *YOR001W* DSB hotspot near *CEN15* (upper panel). Percentage of DSBs over total DNA at the *YOR001W* locus at the indicated time points is shown in the lower panel. The data are mean of two independent biological replicates and error bars represent the range.

Figure6

Enrichment of Hop1 and DSB markers on small chromosomes increases significantly in late prophase and depends on Pch2.

(A-D) Mean ChIP-seq enrichment per Kb is plotted for each chromosome on log scale with regression analysis. *P* and R^2 values are noted below the sample name. R^2, measure of the fit of the points to the line, can vary from 0-1.0 with 1.0 indicating a perfect fit. *P* is the probability of obtaining large R^2 values. ANOVA was performed to test significant difference in the slope between the regression lines for different ChIP-seq samples. ANOVA-derived *P* values are indicated, *** $P < 0.001$. (A) pH2A ChIP-seq enrichment in early (T=3hrs) and late prophase (T=6hrs) in *ndt80Δ* and late prophase (6hrs) in *spo11Δ ndt80Δ*. (B) Hop1 ChIP-seq in early (3hrs) and late prophase (T=6hrs) in *ndt80Δ* samples. (C) Mek1 ChIP-seq in early (T=3hrs) and late prophase (T=6hrs) in *ndt80Δ* cultures. (D) Late prophase (6hrs) enrichment of Hop1 in *ndt80Δ* and *pch2Δ ndt80Δ* cultures.

Figure7

Model - Telomere-adjacent enrichment of Hop1 in late prophase boosts the bias for DSBs and COs on small chromosomes. The orange bars illustrate the large regions (~100 Kb) of long-lived DSB hotspots at telomere-adjacent and rDNA-adjacent domains. Interstitial regions (magenta) harbor mainly the short-lived DSB hotspots.

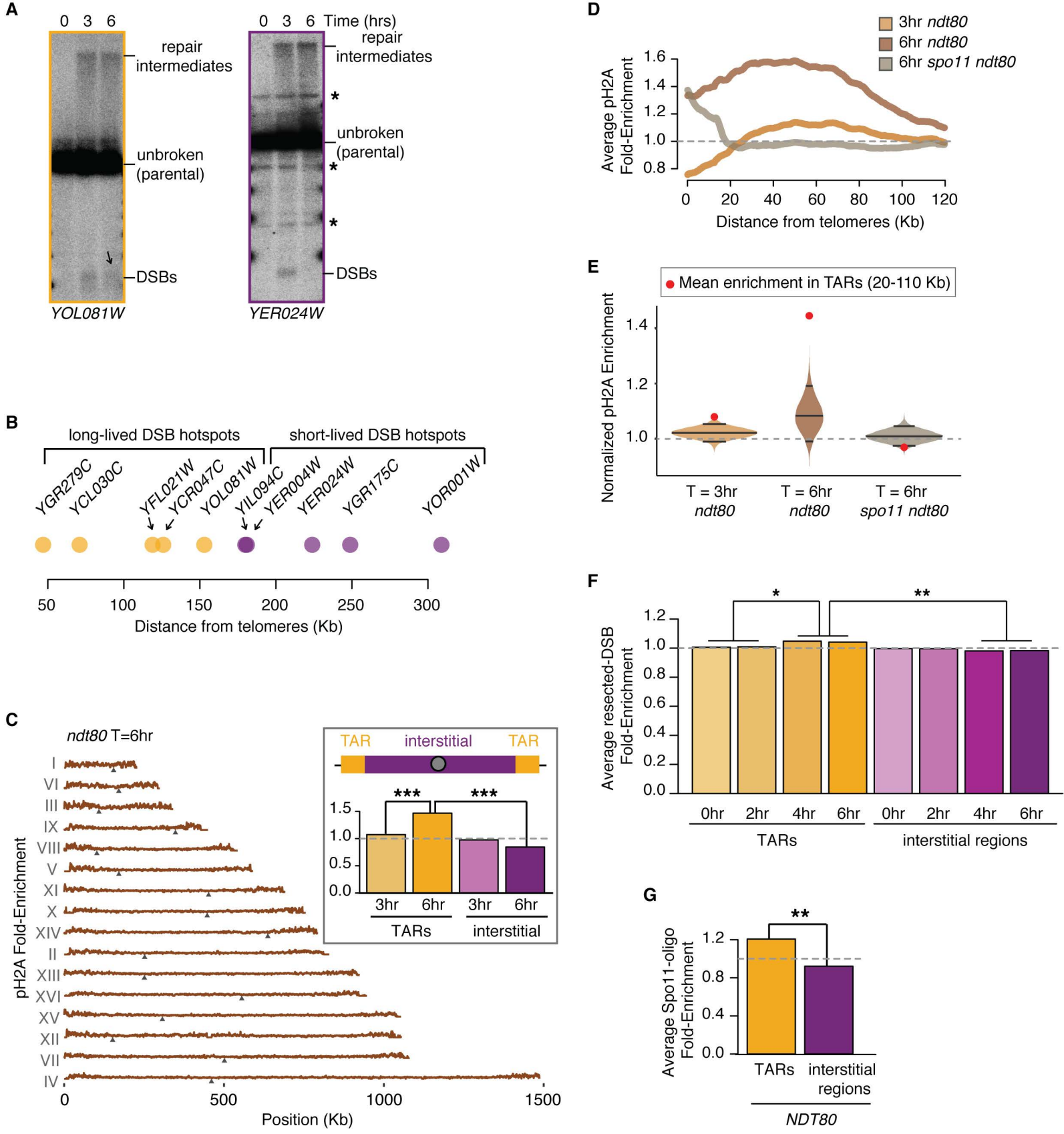

Subramanian *et al.*, Figure 1

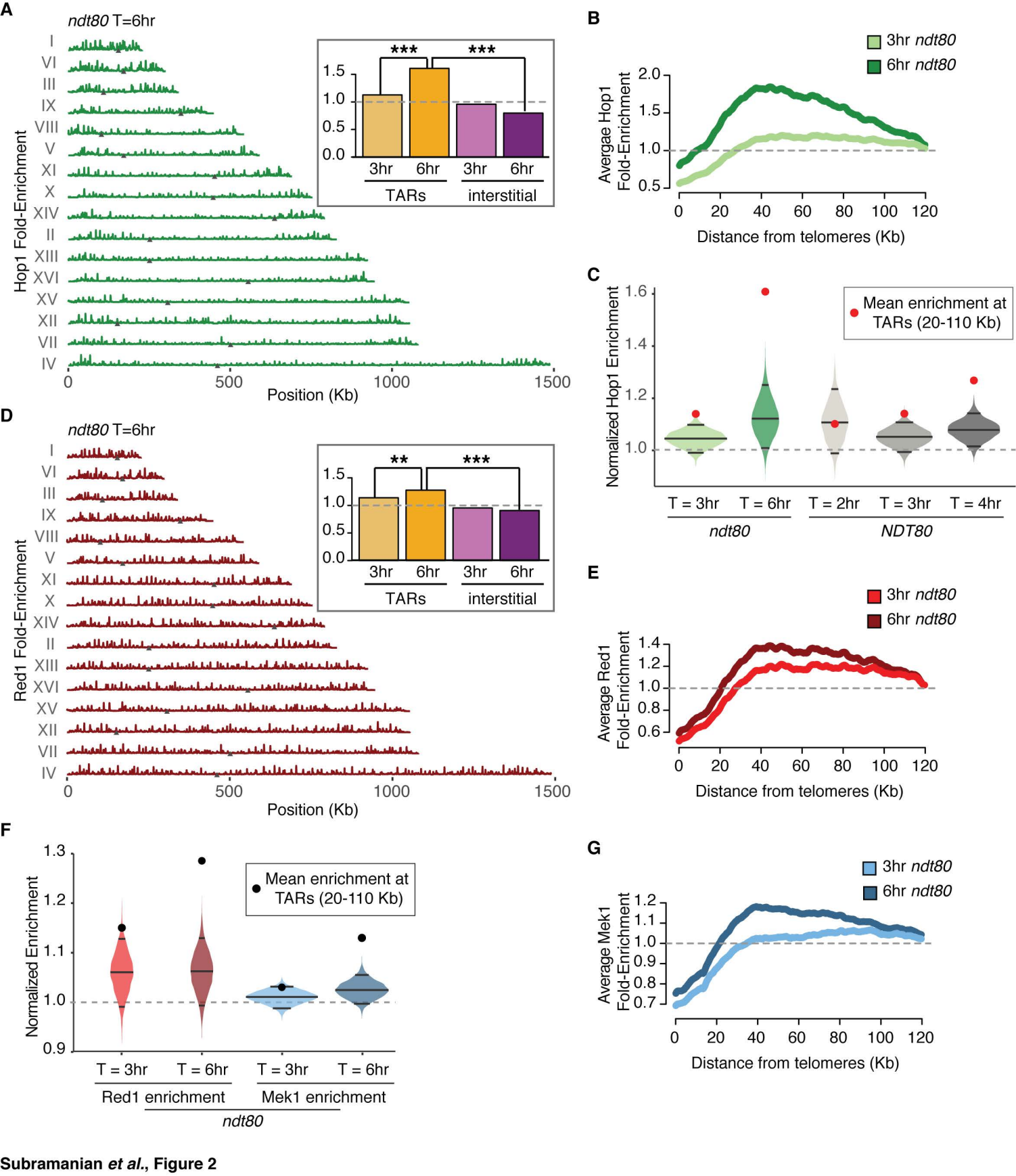

Subramanian *et al.*, Figure 2

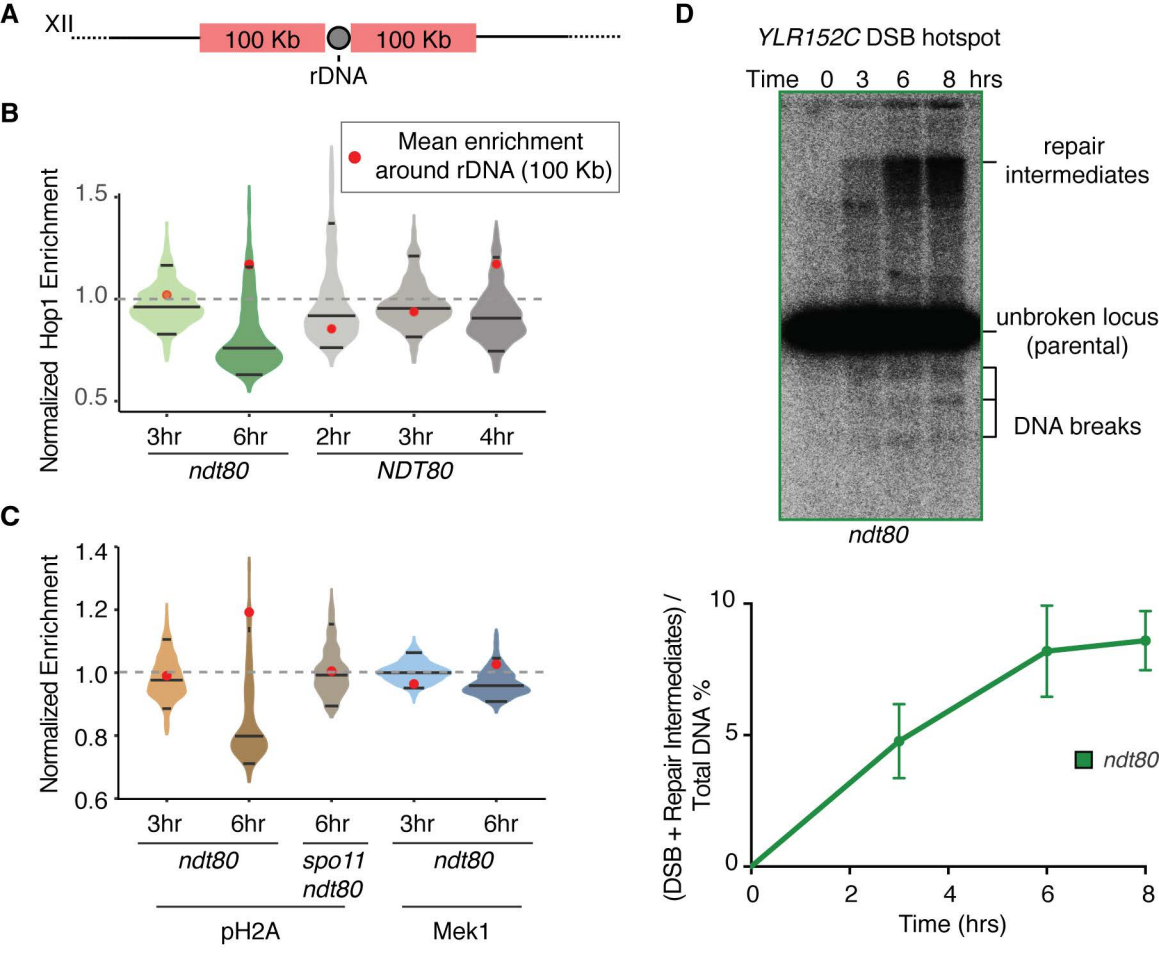

Subramanian *et al.*, Figure 3

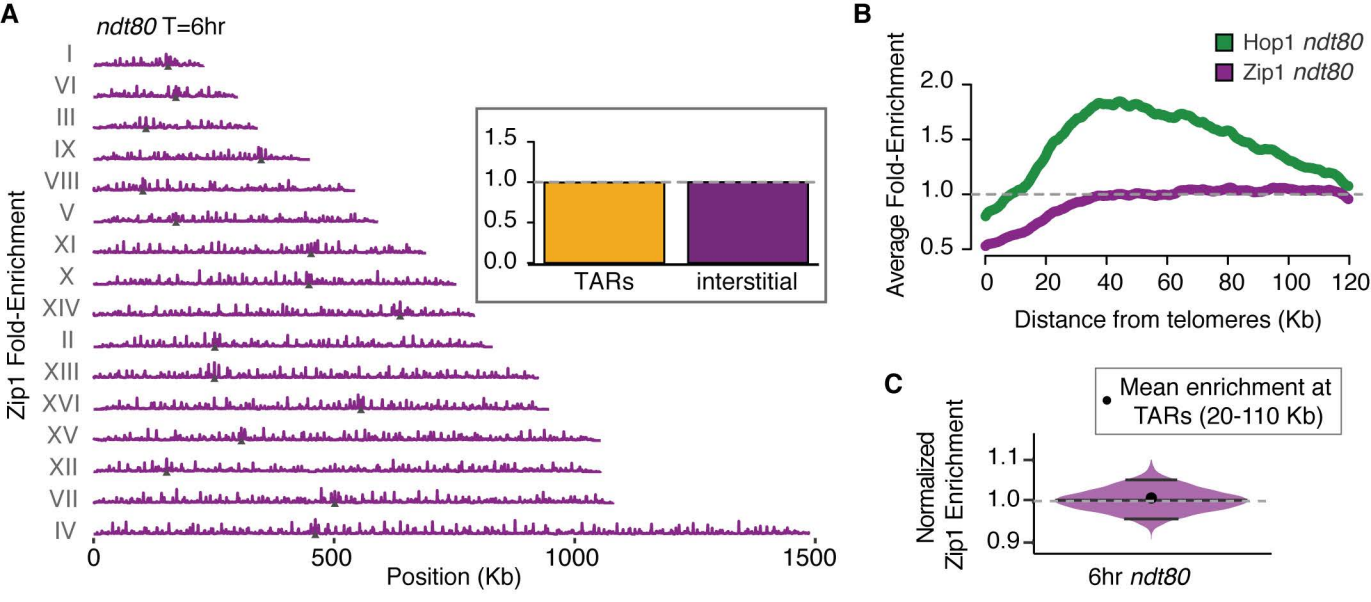

Subramanian *et al.*, Figure 4

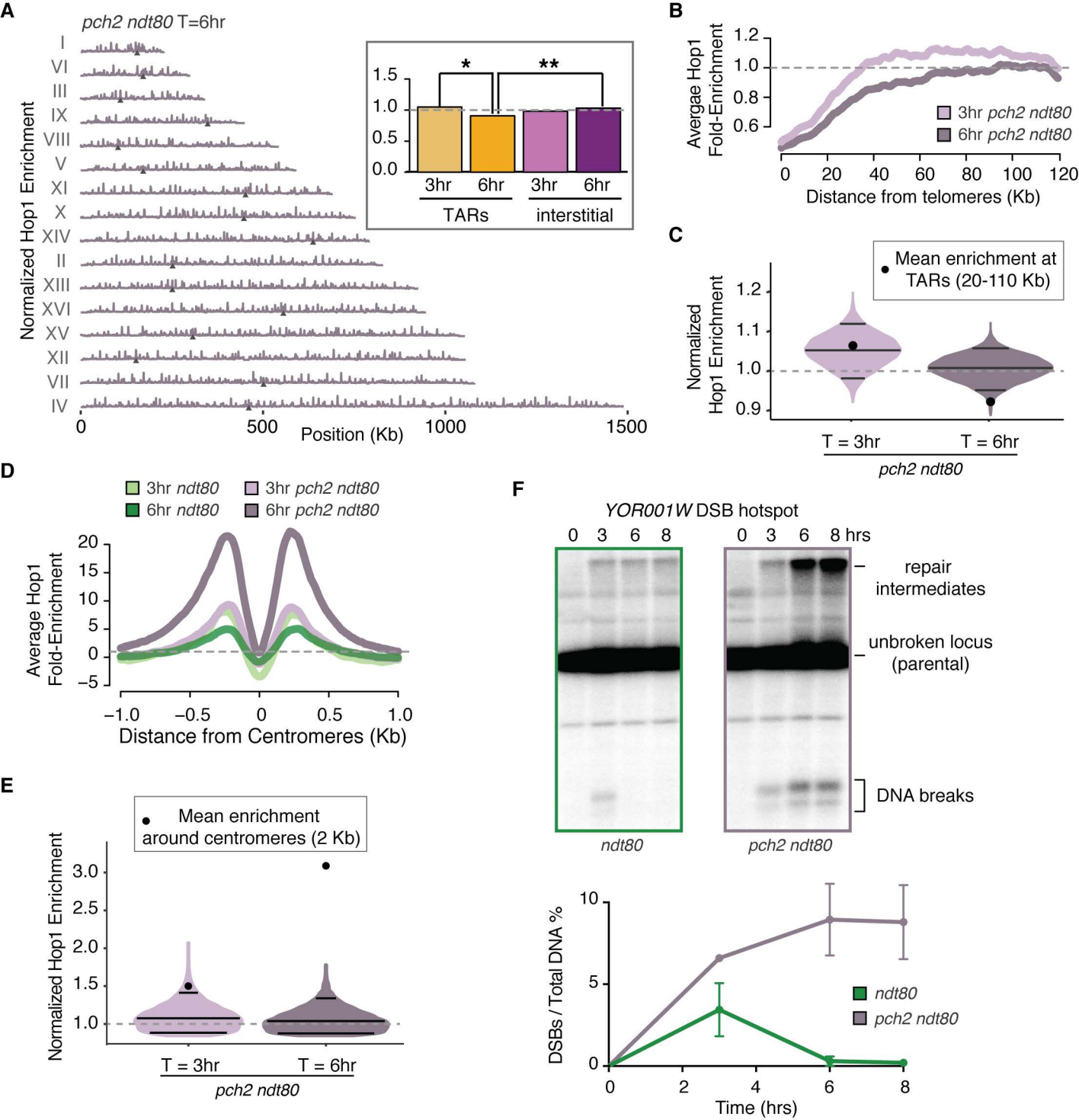

Subramanian *et al.*, Figure 5

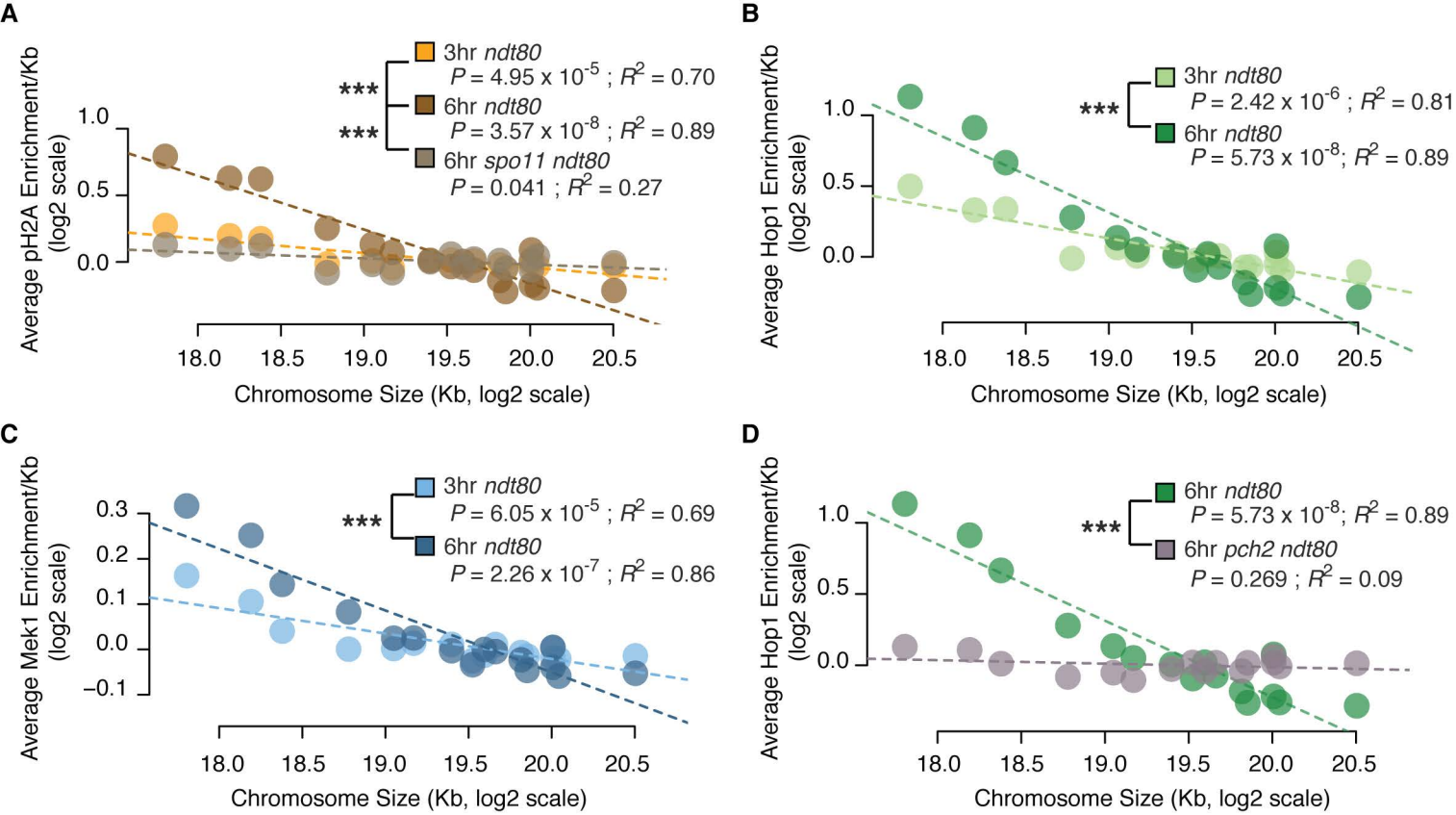

Subramanian *et al.*, Figure 6

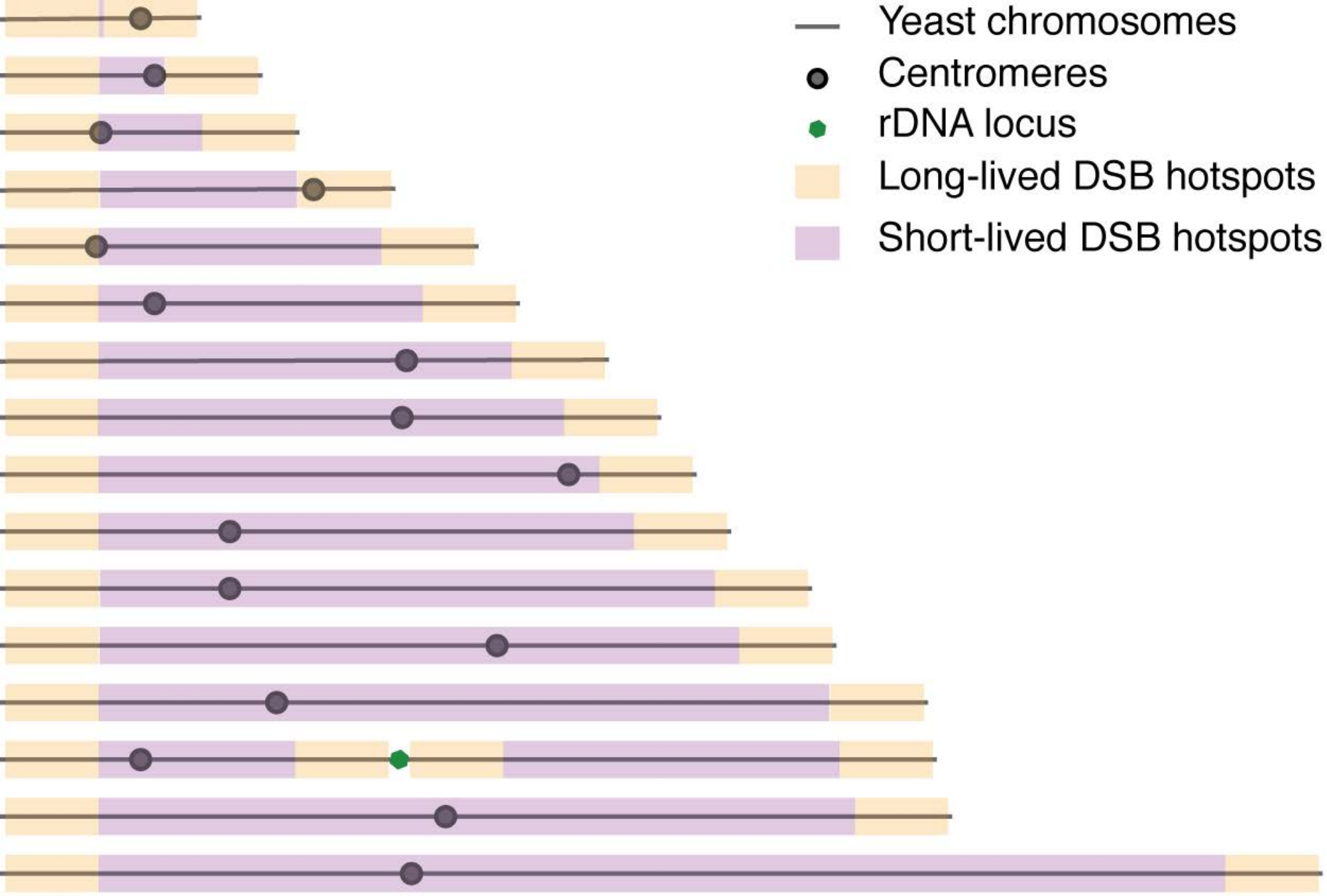

Subramanian *et al.*, Figure 7